MCB
Journals.ASM.org

Cross Talk between CD3 and CD28 Is Spatially Modulated by Protein Lateral Mobility

Keenan T. Bashour,[a] Jones Tsai,[a]* Keyue Shen,[a]* Joung-Hyun Lee,[a] Eileen Sun,[a]* Michael C. Milone,[b] Michael L. Dustin,[c,d] Lance C. Kam[a]

Department of Biomedical Engineering, Columbia University, New York, New York, USA[a]; Department of Pathology and Laboratory Medicine, University of Pennsylvania School of Medicine, Philadelphia, Pennsylvania, USA[b]; Molecular Pathogenesis Program, Skirball Institute of Biomolecular Medicine, New York University School of Medicine, New York, New York, USA[c]; Nuffield Department of Orthopedics and Musculoskeletal Sciences, The University of Oxford, and Kennedy Institute of Rheumatology, Oxford, United Kingdom[d]

Functional convergence of CD28 costimulation and TCR signaling is critical to T-cell activation and adaptive immunity. These receptors form complex microscale patterns within the immune synapse, although the impact of this spatial organization on cell signaling remains unclear. We investigate this cross talk using micropatterned surfaces that present ligands to these membrane proteins in order to control the organization of signaling molecules within the cell-substrate interface. While primary human CD4$^+$ T cells were activated by features containing ligands to both CD3 and CD28, this functional convergence was curtailed on surfaces in which engagement of these two systems was separated by micrometer-scale distances. Moreover, phosphorylated Lck was concentrated to regions of CD3 engagement and exhibited a low diffusion rate, suggesting that costimulation is controlled by a balance between the transport of active Lck to CD28 and its deactivation. In support of this model, disruption of the actin cytoskeleton increased Lck mobility and allowed functional T-cell costimulation by spatially separated CD3 and CD28. In primary mouse CD4$^+$ T cells, a complementary system, reducing the membrane mobility increased the sensitivity to CD3-CD28 separation. These results demonstrate a subcellular reaction-diffusion system that allows cells to sense the microscale organization of the extracellular environment.

Spatial organization plays important roles in cell signaling, governing a wide range of functions, including migration, polarization, and morphogenesis. A striking example at subcellular scales has emerged in the immune synapse (IS), a small (~70-μm^2) area of contact between a lymphocyte and an antigen-presenting cell (APC) which serves as a platform that focuses and modulates cell-cell communication. The archetypal IS formed between a T cell and an APC contains a central supramolecular activation cluster (cSMAC) of T-cell receptor (TCR)—pMHC complexes surrounded by a peripheral supramolecular activation cluster (pSMAC) with LFA-1–ICAM-1 (1–3). The interfaces of different T-cell–APC pairings exhibit variations on this "bullseye" pattern (4–10), and manipulation of IS structure modulates T-cell activation (11–13), suggesting that microscale organization contributes to the language of cell-cell communication. However, the concept that signaling can be modulated at such scales places stringent requirements on the dynamics of intracellular signaling molecules (14–17), and experimental examples of such mechanisms, particularly within the small dimensions of the IS, have been elusive.

We focus here on spatially resolved, microscale cell signaling in the context of CD28 costimulation. When bound by CD80 or CD86, typically presented by an APC in conjunction with pMHC, CD28 augments TCR signaling and is essential for full activation of naive T cells. A role of spatial organization in this signaling was established by experiments in which CD28 was engaged outside the IS, a *trans*-costimulation configuration representing the action of a bystander cell auxiliary to the main T-cell–APC interaction (18–22). This configuration can lead to cellular activation, but through different mechanisms than the *cis*-costimulation configuration, in which CD28 is engaged within the IS, along with TCR; interleukin-2 (IL-2) secretion is enhanced in *trans* costimulation by stabilization of mRNA, while the *cis* configuration involves higher levels of transcription (18–22). Subsequent studies suggested a role of spatial organization within the IS in CD28 costimulation. CD28 initially comigrates with TCR in microclusters from the IS periphery but separates from these structures at the pSMAC-cSMAC boundary (23, 24), which correlates with increased T-cell activation in mouse cells (25). In this report, we show that microscale separation of CD28 from CD3 within the IS modulates activation of primary human CD4$^+$ T cells, leading to a new model of spatially resolved intracellular signaling involving the convergence of two signaling pathways. We further propose that the lateral mobility and dynamics of intermediate signaling molecules allows cells to recognize microscale organization of CD3 and CD28 and focus on Lck, a major Src family kinase expressed in T cells, as a representative example of this mechanism. Lck is critical for TCR triggering and downstream signaling but also phosphorylates and activates CD28 (26, 27). In addition, Lck activity and presence within the immune synapse is under the control of CD3 and CD28 (28–30). Together, these intercon-

Received 28 June 2013 **Returned for modification** 21 September 2013
Accepted 21 December 2013

Published ahead of print 30 December 2013

Address correspondence to Lance C. Kam, lk2141@columbia.edu.

* Present address: Jones Tsai, Department of Pharmaceutical Sciences, University of California, Irvine, California, USA; Keyue Shen, Center for Engineering in Medicine, Massachusetts General Hospital, Harvard Medical School, Boston, Massachusetts, USA; Eileen Sun, Department of Virology, Harvard University, Boston, Massachusetts, USA.

doi:10.1128/MCB.00842-13

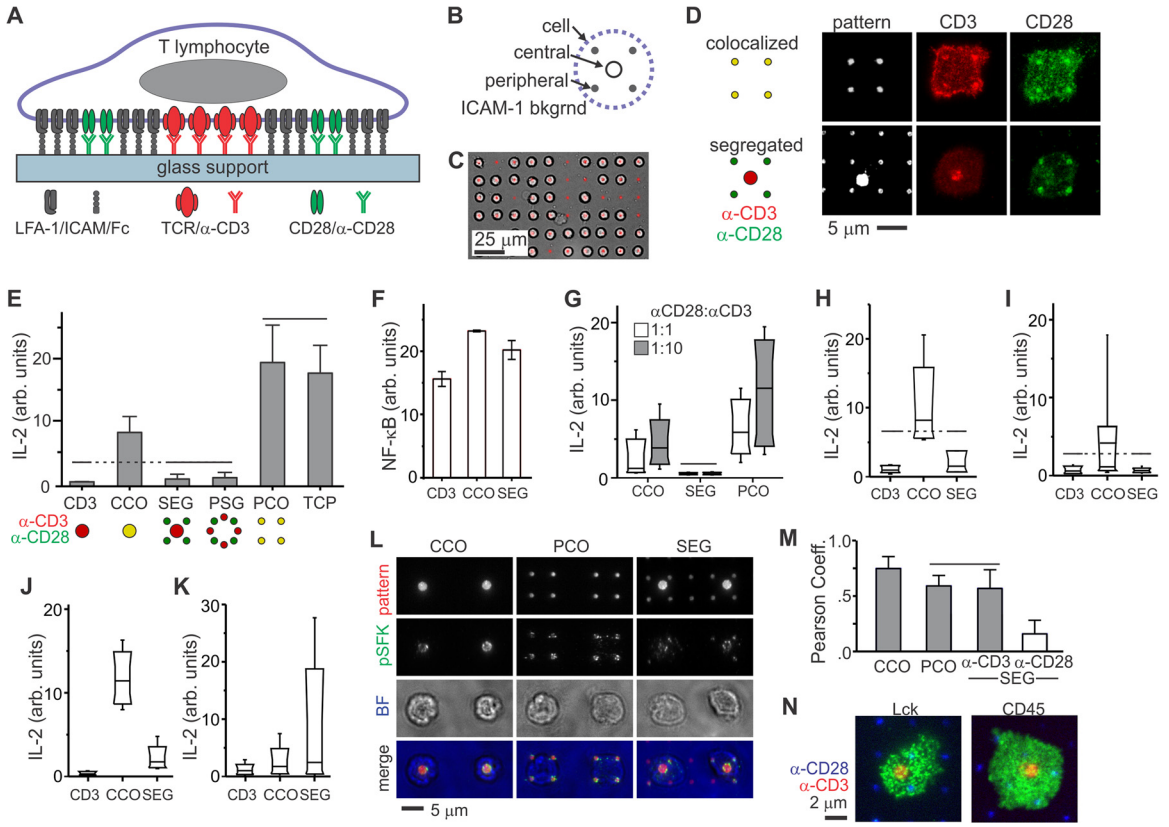

FIG 1 Primary human CD4$^+$ T cells from peripheral blood sense the microscale separation of CD3 and CD28 signaling. (A) Micropatterned surfaces provide control over the molecular organization of an artificial synapse. (B) Layout of an individual costimulation site. (C) Long-range arraying of primary human T cells on micropatterned surface, 30 min after initiation of cell-surface contact. (D) Local, microscale control over the layout of TCR (CD3) and CD28 within artificial immune synapses by patterning of anti-CD3 (OKT3) and anti-CD28 (9.3). These cells were fixed and stained 30 min after initiation of cell-surface contact. (E) IL-2 secretion was curtailed by separation of CD3 and CD28 engagement by micrometer-scale distances. TCP = antibody coated tissue culture plastic. The data are means ± the SD from >2,000 cells per surface (n = 5 independent experiments) and were compared by using ANOVA/Tukey methods; overbars group conditions that are not statistically different ($\alpha = 0.05$). (F) Translocation of NF-κB in response to surface patterning. The data represent mean ± the SD. from three independent experiments, representing 17 to 25 cells per sample. Each condition was statistically different from all others (ANOVA/Tukey multiple comparison, $\alpha = 0.05$). (G) Changing the relative concentrations of OKT3 and 9.3 in the micropatterning process did not alter the sensitivity of human CD4$^+$ T cells to segregated costimulation. The standard ratio of OKT3 to 9.3 is 1:3. The data are box plots from a representative experiment, representing more than 2,000 cells per surface, and compared using ANOVA/Tukey methods ($\alpha = 0.05$). (H and I) Replacing OKT3 with HIT3a (H) or 9.3 with CD28.6 (I) did not change the sensitivity of cells to segregated patterns. The data are box plots from representative experiments (n > 2,000 cells for each condition) and were analyzed using Kruskal-Wallis/Tukey methods ($\alpha = 0.05$). (J and K) Comparison of IL-2 secretion by CD4$^+$ T cells from human umbilical cord blood (J) and mouse peripheral blood (K). The data represent >2,000 cells for each condition from a representative experiment. Within each experiment, each condition was statistically different from all others, as analyzed using Kruskal-Wallis/Tukey methods ($\alpha = 0.05$). (L) Activated Lck in primary human CD4$^+$ T cells is tightly associated with features of anti-CD3. Cells were stained 15 min after initiation of cell-substrate contact. Pattern, anti-CD3 and anti-CD28; pSFK, anti-pY394; BF, bright field. (M) Quantitative comparison of pLck correlation with anti-CD3 and anti-CD28. The data represent means ± the SD for 10 to 15 cells on each pattern. The data were analyzed by ANOVA/Tukey methods ($\alpha = 0.05$). (N) Total Lck and CD45 were uniformly distributed across the cell-surface interface. These representative cells were fixed 15 min after substrate contact.

nected roles place Lck in a strategic position for coordinating CD3 and CD28 signaling.

MATERIALS AND METHODS

Substrate preparation. Borosilicate glass coverslips were patterned by microcontact printing using previously described techniques (13) that were further adapted for use here with human cells. Surfaces contained arrays of costimulatory sites, spaced at 15- and 12-μm intervals for human and mouse cells, respectively. These dimensions were chosen for each cell type to allow spreading across an individual site while limiting interaction with multiple sites and reflect the larger size of human versus mouse cells. Each site consisted of anti-CD3 and anti-CD28 antibodies arranged in two basic motifs or a combination of these (Fig. 1B). The first is a single, 2-μm-diameter circle targeting the center of the cell surface IS, while the second is a cluster of 1-μm-diameter dots placed in the interface periphery. The clustered dots are spaced at center-to-center distances of 5 and 4 μm for human and mouse cells, respectively, such that a typical T cell will interact with four features thus presenting the same area as a single 2-μm-diameter circle. For each step, stamps were coated with a mix of species-specific anti-CD3 and anti-CD28 antibodies totaling 25 μg/ml. Unless otherwise specified, colocalized patterns were created using stamps coated with a 1:3 mass ratio mix of OKT3 (Janssen-Cilag or Biolegend) to 9.3 (prepared in-house) for experiments with human cells or a 1:10 mix of clone 145-2C11 to clone 37.51 (eBioscience) for mouse cells. Segregated patterns were made by combining separate steps for anti-CD3 and anti-C28 on the same substrate, replacing the other active antibody in the mix with a nonreactive counterpart. TS2/4 (ATCC) and goat anti-rat IgG (Invitrogen) were used for experiments targeting mouse and human cells, respectively. Substrates were then coated with

2 μg of species-specific ICAM/Fc/ml for 2 h; this protein consisted of the extracellular domain of ICAM-1 fused with the Fc region of human IgG (R&D Systems).

The microcontact printing conditions used here deposits 200 antibodies/μm^2 (13), consistent across the antibodies included here. Coating a stamp with a mix of antibodies splits the resultant surface concentration proportionally; the standard 1:3 mass-ratio mix of OKT3 and 9.3 produced surface concentrations of 50 and 150 molecules/μm^2 (31). The CD3, CCO, and PCO patterns were created in one step, while SEG and PSG were created by sequentially stamping anti-CD28 and anti-CD3 onto the same surface. For mouse cells, PCO patterns were created using the repeating pattern of 1-μm dots used in the SEG pattern; cells on these surfaces typically interacted with one group of four of these smaller features. In specific experiments, cholera toxin subunit B (CTX) or bovine serum albumin was mixed with ICAM/Fc at a mass ratio of 1:5; yielding similar surface concentrations of ICAM/Fc.

T cells. Human $CD4^+$ T cells were purified from peripheral blood lymphocyte fractions by negative selection (Rosette-Sep method; Stem Cell Technologies). These preparations contained >95% $CD4^+$ cells, predominantly a mix of naive and memory phenotypes. Mouse $CD4^+$ T cells were isolated from lymph nodes of C57BL/6 animals by bead-based, negative selection (Dynal beads; Invitrogen). These preparations contained >85% naive cells ($CD44^+/CD62L^-$). Primary human T cells were either isolated from leukopacks or provided by the Immunology Core of the University of Pennsylvania Gene Therapy Program without information identifying the specific donor. For indicated experiments, mouse $CD4^+$ T cells were isolated from peripheral blood lymphocyte fractions by negative selection, while T cells from human cord blood were obtained from the University of Pennsylvania Immunology Core. For all experiments, cells were resuspended in RPMI (Invitrogen) plus 5% serum (fetal bovine and mouse serum for human and mouse experiments, respectively) and seeded onto surfaces at a density of 2×10^4 cells/mm^2. To inhibit cytoskeletal dynamics in specified experiments, medium containing 1 μM latrunculin B (LatB; Sigma-Aldrich) was washed within 15 min following initiation of cell-substrate contact and incubated under standard cell culture conditions in this medium for an additional 15 min before analysis. All animal procedures were carried out in accordance with protocols approved by the Columbia University Institutional Animal Care and Use Committee.

Image acquisition. All images were collected using an Olympus IX81 inverted microscope in epifluorescence, total internal reflection fluorescence (TIRF), or transmitted light mode. All images were collected using either a Hamamatsu C9100-02 EMCCD or Andor Neo sCMOS camera. A custom-built launch apparatus was used to place a diffraction-limited spot of laser-sourced light in the microscopy field of view for photobleaching experiments, the analysis of which is described below. Measurements of protein diffusion were carried out at 37°C in a 5% CO_2–95% air mixture (LiveCell, Pathology Devices, environmental chamber) with phenol red-free RPMI as the culture medium. For comparisons of protein staining intensity, all conditions were included in each experiment. All samples in each experiment were prepared, stained, and imaged in the same session. Fluorescence linearity was verified using InSpek calibration beads (Invitrogen), but data were normalized across experiments by allowing a proportional change in signal (due to staining efficiency or microscopy sensitivity that could vary session-to-session) as previously described (13, 32). All images were collected and analyzed using the MetaMorph and ImageJ imaging suites.

Immunostaining. For receptor localization, cells were fixed and stained 30 min after seeding with antibodies to CD3 (ab5690; Abcam) and CD28 (sc-1624; Santa Cruz Biotechnology) and then imaged by total internal reflection fluorescence microscopy (TIRFM). Additional visualization was done with antibodies for total Lck (v49; Cell Signaling Technology), pY394 Lck (pSFK, NB100-82019; Novus Biologicals), CD45 (catalog no. 304019; Biolegend), and F-actin (phalloidin; Invitrogen). Images of these signals were obtained by TIRFM. Surface patterns were visualized by fluorescently labeling a fraction (20%) of the activating antibodies used in microcontact printing (13). Nuclear translocation of NF-κB (detected 4 h after seeding with antibody clone sc109 [Santa Cruz Biotechnology]) was quantified by taking image stacks through adherent cells and collecting the signal associated with the nucleus interior, as previously described (13).

IL-2 assay. Secretion of IL-2 was measured by using a commercially available, surface capture system designed for flow cytometric analysis (Miltenyi Biotec). Briefly, cells were incubated prior to seeding with an IL-2 capture reagent that binds to the cell surface. Cells were then seeded onto prepared surfaces in RPMI plus 5% fetal bovine serum (FBS). At 6 h after seeding, the cells were rinsed and labeled with a fluorescently tagged antibody to IL-2 (the detection reagent of the kit) and then fixed. Surface-captured IL-2 was estimated by microscopy and typically exhibited a single, non-Gaussian peak on each surface as previously described (13). The average fluorescence intensity across all cells observed on a surface was used to represent that surface in comparisons across multiple experiments and patterns.

Diffusion coefficient. A plasmid vector (Lck-YFP) encoding full-length Lck (33) appended (C terminus) with EYFP was introduced into primary mouse and human T cells using the AMAXA nucleofection system, following the manufacturer's instructions and associated reagents indicated for primary T cells. Cells were allowed to rest overnight after transfection in RPMI plus 5% FBS and then seeded onto glass surfaces that were previously coated for 2 h with a mix of 5 μg of anti-CD3/ml plus 5 μg of anti-CD28/ml and 2 μg of ICAM/Fc/ml. At 1 h after seeding, fluorescence recovery after photobleaching (FRAP) experiments were carried out using a laser to photobleach a small, micrometer-scale spot in the middle of the cell-substrate interface. Time series images of Lck-YFP recovery in the cell-substrate interface were then collected using TIRFM. The diffusion coefficient of Lck was estimated from these image sets as described by Hook and coworkers (34). This FRAP algorithm uses low-wavenumber components of the Bessel transform of data from each time point to estimate diffusion coefficient. By focusing on these transforms, this approach is insensitive to punctate distributions of signal and does not require a specific initial profile, such as a top-hat or Gaussian distribution.

Statistics. Comparisons of data over multiple conditions were carried out using analysis of variance (ANOVA) and Tukey significant difference methods. In the case where data were not normally distributed, as determined using a Lillifors test, Kruskal-Wallis approaches were used in place of ANOVA. Unless otherwise specified, plots of data that were analyzed with Tukey methods group conditions that are not statistically different from each other by overbars, with dotted lines connecting overbars of the same group. Comparisons between data consisting of only two conditions were carried out using dual-tailed *t* test or Kruskal-Wallis approaches. Unless otherwise specified, a value of $\alpha = 0.05$ was chosen to determine statistical significance. For box plots representing >100 data points per condition, the whiskers and elements of the hourglass-shaped boxes represent the following percentiles: 95, 90, 75, 50, 25, 10, and 5. For box plots representing <100 data points, the whiskers and parts of the rectangular boxes represent the following percentiles: 90, 75, 50, 25, and 10. Statistical analyses were carried out using MATLAB (Mathworks) or Origin (OriginLab) software.

RESULTS

Primary human T cells are sensitive to microscale separation of CD3 and CD28. The microscale organization of CD3 and CD28 signaling was controlled in the present study by replacing the APC with a substrate containing multiple, independent patterns of ligands to these membrane proteins. Specifically, planar glass substrates were patterned with costimulation sites (Fig. 1A) containing the antibodies OKT3 and 9.3, which activate human CD3 (epsilon subunit, a key signaling component of the TCR) and CD28, respectively (13, 35, 36). Each site consisted of antibodies

arranged in a single 2-μm-diameter circle targeting the center of the cell-substrate interface, a cluster of four 1-μm, peripheral dots, or a combination of these two motifs (Fig. 1B). The areas surrounding and separating the OKT3 and 9.3 features were backfilled with ICAM/Fc. These patterns were effective in directing both the long-range order of T cells on the substrates (Fig. 1C) and the local organization of CD3 and CD28 receptors within individual cell-substrate interfaces (Fig. 1D). Complete details of this system, including methods used to normalize the protein concentrations in each pattern, are included in a previous report (13) and are summarized in Materials and Methods.

Stimulation of human $CD4^+$ T cells with patterns containing colocalized OKT3 and 9.3 (CCO and PCO, which target the center and periphery of the cell-substrate interface, respectively) resulted in strong activation of cells, as measured by a 6-h secretion of IL-2, a high-level function reflecting cellular activation (Fig. 1E); this readout has proven to be a useful, graded response of cells to substrates (13, 32). Furthermore, presenting colocalized OKT3 and 9.3 in the periphery of the cell-substrate interface (PCO) promoted greater IL-2 secretion than in the center (CCO), reaching a level comparable to uniformly coated surfaces (Fig. 1E). This is consistent with earlier reports that maintaining signaling complexes in the IS periphery enhances activation (12, 13). In sharp contrast to the colocalized patterns, IL-2 secretion was abrogated on patterns for which OKT3 and 9.3 were separated by microscale distances. One pattern consisted of a central OKT3 feature surrounded by four peripheral regions of 9.3 (SEG, Fig. 1E), while the other contained these antibodies in separate features in the interface periphery (PSG). IL-2 secretion on these surfaces was similar to that on patterns for which anti-CD28 was omitted (CD3 pattern, Fig. 1E), indicating a lack of functional CD28 costimulation. These changes in IL-2 secretion were mirrored by NF-κB translocation; intranuclear staining for this transcription factor was significantly higher on the CCO surface than the SEG or CD3 patterns (Fig. 1F). Importantly, the effects of microscale organization were not limited to these specific patterning parameters. Increasing the surface concentration of either CD3 or CD28 by changing the ratio of OKT3 to 9.3 used in patterning did not rescue IL-2 secretion on the SEG pattern (Fig. 1G). Replacing OKT3 with HIT3a (Fig. 1H) or 9.3 with CD28.6 (Fig. 1I) similarly did not alter the pattern of IL-2 secretion. A surprising aspect of these responses is that they contrast sharply with that of primary naive $CD4^+$ T cells from mouse lymph nodes, which we previously showed are not sensitive to microscale separation of CD3 and CD28 engagement (13). To better understand the factors controlling these responses, the response of IL-2 secretion by cells from two additional sources was examined. Human cells isolated from umbilical cord blood (which are predominantly naive) show sensitivity to CD3-CD28 separation that is similar to that seen for resting cells from peripheral circulation (Fig. 1J), while those from mouse peripheral blood are similar to cells from mouse lymph nodes (Fig. 1K). These results indicate that differences between human peripheral blood resting cells and mouse lymph node naive cells, which are the focus of the remainder of this report, are not restricted to these specific preparations. Below, these two systems are referred to by species for brevity, but it is recognized that this delineation is simplistic and that additional factors may affect how cells from any given preparation behave. However, we first sought to understand how the human cells can sense the separation/colocalization of CD3 and CD28, focusing on Lck as an intermediary signaling protein.

Phospho-Lck is localized around sites of CD3 engagement in human $CD4^+$ T cells. The multiple roles that Lck has in regulating signaling by the TCR complex and CD28 suggests that this kinase may play important roles in coordinating their interaction. Activation of Lck is dependent on phosphorylation at Y394. Immunostaining with a phospho-specific antibody for this site in cells fixed 15 min after seeding showed sharp enrichment at features containing OKT3 on the CCO, PCO, and SEG patterns (Fig. 1L); it is noted that current antibodies cannot distinguish between Y394 on Lck and the homologous site Y417 of Fyn, so this signal is denoted as pSFK. Focusing on the SEG pattern, pSFK showed higher correlation with features of OKT3 than 9.3 (Fig. 1L and M), suggesting a mechanism for spatial regulation of costimulation. Specifically, the ability of Lck to act on CD28 and induce downstream signaling in this system is determined by the microscale overlap between sites of CD3 and CD28 engagement, since localization of active Lck follows that of CD3. As a mechanism for this localization, we first examined the distribution of total Lck. Staining with a non-phospho-specific antibody revealed that Lck was distributed across the entire cell-substrate interface (Fig. 1N), and the per-area intensity of Lck staining was not statistically different between CCO and SEG surfaces; 1.00 ± 0.22 versus 0.96 ± 0.24, respectively (data are means ± the standard deviations [SD] of arbitrary fluorescence units per area normalized to the CCO surface, $n > 18$ cells per surface, collected over three independent experiments, $P < 0.66$ as determined by two-way ANOVA). This suggests that the differences in pSFK distribution and cell response are due to regulation of Lck activity rather than recruitment or exclusion of Lck from the cell-surface interface. A potential mechanism for this regulation is differential exclusion of CD45, which dephosphorylates active Lck, from the T-cell–substrate interface as a function of surface pattern (37, 38). However, CD45 was distributed across the cell-substrate interface on both CCO and SEG patterns with little large-scale exclusion (Fig. 1N). The fluorescence intensity associated with CD45 staining was higher on CCO patterns compared to SEG surfaces (1.00 ± 0.43 versus 0.70 ± 0.20, respectively, $P < 0.05$, $n > 16$ cells per surface, collected over three independent experiments). However, this would not explain the stronger activation on CCO patterns, since higher CD45 levels would be associated with stronger Lck deactivation and lower cell activation, in contrast to the results shown in Fig. 1E.

The IS cytoskeleton reduces Lck mobility and confers spatial sensitivity in human T cells. As an alternative mechanism for regulating Lck activity, we measured the mobility of Lck across the cell-substrate interface. A vector encoding Lck-YFP was transfected into primary human cells that were subsequently seeded onto surfaces uniformly coated with a mix of OKT3, 9.3, and ICAM1/Fc. The long-range diffusion coefficient of Lck-YFP, as well as mobile fraction of this protein, was estimated from fluorescence recovery profiles after local photobleaching by a focused laser spot placed in the cell-substrate interface (Fig. 2A and B). Laterally mobile Lck was found across the cell-substrate interface and comprised 60% of the total observed protein, superimposed against a number of immobile features, which are potentially endosomes within the TIRFM evanescent field (Fig. 2A, but are also visible in Fig. 1N). Mobile Lck-YFP exhibited a diffusion coefficient of 0.04 ± 0.02 $\mu m^2/s$ (Fig. 2C, mean ± the SD), lower than

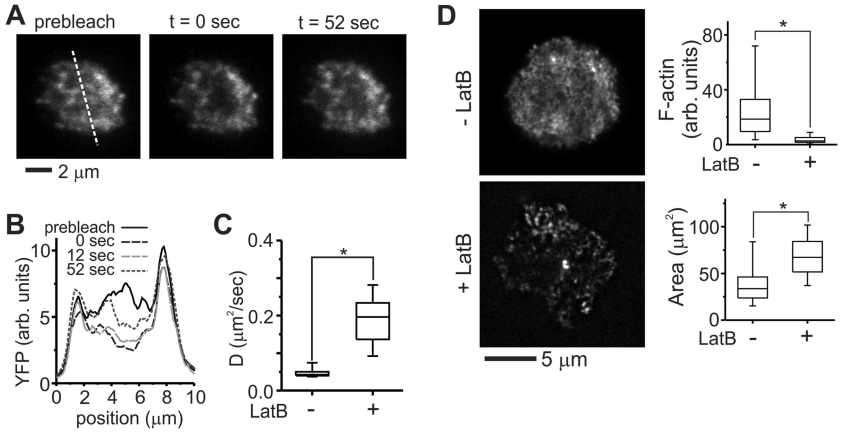

FIG 2 The IS cytoskeletal network hinders mobility of membrane proteins. (A) The long-range diffusion coefficient of Lck was estimated by FRAP. This series of images illustrates the distribution of Lck-YFP before, immediately after, and 52 s after photobleaching. (B) Line profiles of Lck-YFP taken across the dotted line indicated in panel A, illustrating recovery of Lck-YFP. (C) Comparison of long-range Lck-YFP mobility in human $CD4^+$ T cells with or without wash-in of 1 μM LatB. The data are box plots from a representative experiment, 7 to 15 cells per condition, and were compared using Kruskal-Wallis methods (*, $P < 0.005$). (D) LatB treatment disrupted a dense F-actin network at the cell-substrate interface. Cells were fixed 30 min after seeding. Each image was individually adjusted for brightness and contrast to allow visualization of F-actin structures and are thus not comparable on a quantitative basis. F-actin staining is compared quantitatively in the top graph, whereas the lower one compares cell spreading in response to LatB wash-in. The data for both graphs are box plots from a representative experiment, >17 cells per condition. The data were compared using Kruskal-Wallis methods (*, $P < 0.005$).

expected for a freely mobile membrane component and also less than that reported for Lck in Jurkat cells (39, 40). When balanced against the deactivation of Lck by membrane-bound phosphatases such as CD45, this low mobility provides a potential mechanism for the concentrations of pSFK observed around features of anti-CD3, as will be detailed later in the Discussion.

To explain this low mobility, we turned to a model by Ike et al. (41) in which TCR-induced polymerization of the cytoskeleton can reduce long-range diffusion of membrane molecules. Phalloidin-based staining revealed an extensive F-actin network in human T cells 30 min after contact with substrates coated with OKT3, 9.3, and ICAM/Fc (Fig. 2D). The effect of this network on Lck mobility was tested by wash-in of latrunculin B (LatB) 15 min after contact with the substrate, allowing cells to undergo initial activation and establishment of an immune synapse prior to treatment. A moderate concentration of LatB (1 μM) was chosen that remained effective in disrupting the cytoskeleton network but avoided completely collapsing the cell-surface contact area (Fig. 2D). The cell area increased upon LatB treatment (Fig. 2D), possibly reflecting reduced cytoskeletal tension and resultant increase in cell spreading.

This disruption had a dramatic effect on Lck mobility and signaling in primary human T cells. The long-range diffusion coefficient of Lck-YFP increased 5-fold compared to untreated cells (Fig. 2C). On patterned surfaces, wash-in of LatB disrupted the cell cytoskeleton similarly to that observed on the coated surfaces (Fig. 3A) but also decreased correlation between pSFK and features of OKT3, indicating a more uniform distribution across the

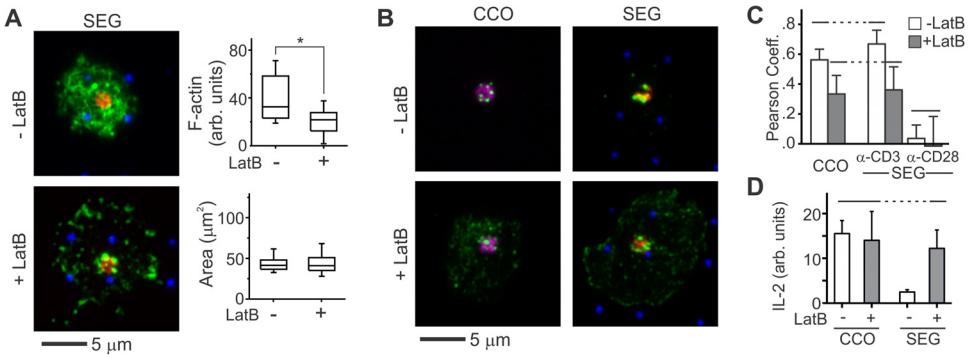

FIG 3 Increased mobility of membrane proteins allows primary human T cells to respond to segregated patterns. (A) LatB wash-in disrupts the IS cytoskeleton and decreases localization of pSFK to OKT3-containing features on micropatterned surfaces. These images illustrate primary human T cells 30 min after seeding on a SEG patterned surface and show anti-CD3 (red), anti-CD28 (blue), and F-actin (green). The graphs quantitatively compare per-area actin intensity and cell spreading. The data are from a representative experiment ($n > 20$ cells per surface). The data were compared using Kruskal-Wallis methods (*, $P < 0.005$). (B) LatB wash-in also changed the distribution of pSFK (green) within these cells. These images illustrate cells 30 min after seeding on CCO and SEG patterns. Areas of anti-CD3 and anti-CD28 are shown in red and blue, respectively, while colocalized patterns appear in purple. (C) Wash-in of LatB changes pLck correlation with anti-CD3 and anti-CD28. The data represent means ± the SD for 10 to 15 cells on each pattern. The data were analyzed using ANOVA/Tukey methods ($\alpha = 0.05$). (D) IL-2 secretion on segregated but not colocalized patterns is enhanced by application of LatB. The data are means ± the SD from three experiments and were analyzed using ANOVA/Tukey methods ($\alpha = 0.05$).

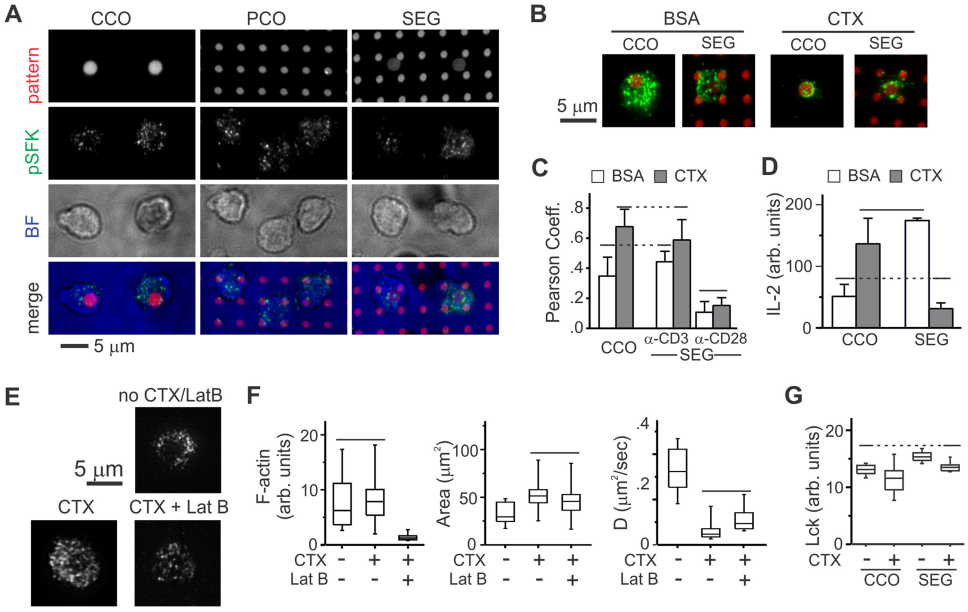

FIG 4 The response of primary mouse cells to micropatterned costimulation is consistent with a diffusion-based model. (A) Staining for pSFK in primary mouse cells is spread across the cell-substrate interface. Cells were fixed 15 min after contact with the substrate. Pattern, anti-CD3 and anti-CD28; pSFK, anti-pY394; BF, bright field. (B) Inclusion of CTX on the substrate surface increases localization of pSFK to anti-CD3 features. In these images, anti-CD3 and anti-CD28 in the CCO and SEG patterns are shown in red, whereas pSFK is in green. (C) Quantitative comparison of the effect of CTX on localization of pSFK. The data are means ± the SD from 10 to 15 cells per condition and were compared by ANOVA/Tukey methods ($\alpha = 0.05$). (D) Comparison of IL-2 secretion as a function of pattern and CTX. The data are means ± the SD across three experiments, which were analyzed using ANOVA/Tukey methods ($\alpha = 0.05$). (E) Actin structure as a function of surface-immobilized CTX and LatB wash-in. These images were individually adjusted for brightness and contrast to allow visualization of F-actin structures. (F) Quantitative comparison of F-actin staining intensity, cell spreading, and Lck-YFP diffusion coefficient as a function of CTX and LatB. In each representative experiment, data are from 8 to 16 cells per surface and were compared using Kruskal-Wallis/Tukey methods ($\alpha = 0.05$). (G) Comparison of average Lck signal in the cell-substrate interface as a function of pattern and CTX inclusion. The data for this representative experiment are from 12 to 49 cells per condition and were compared using ANOVA/Tukey methods ($\alpha = 0$ 0.05).

cell (Fig. 3C). Localization of pSFK relative to 9.3 was unchanged by LatB wash-in and remained largely uncorrelated with these sites of CD28 engagement. It is noted that 9.3 and OKT3 comprise a small fraction of the surface (ca. 5% each of a typical cell-substrate interface). The lack of change in pSFK correlation with anti-CD28 suggests that phospho-Lck has a similar affinity for antibody-bound CD28 and the surrounding, ICAM/Fc-coated areas; although the amount of phospho-Lck interacting with areas away from OKT3 is increased upon LatB treatment, increases at these sites of CD28 engagement are difficult to detect because of the small area associated with 9.3. Finally, the application of LatB allowed cells to respond to segregated patterns of OKT3 and 9.3, as reflected by increased IL-2 secretion on these surfaces (Fig. 3D). These results all support a role of Lck in spatially mediating cross talk between CD3 and CD28, with the cell cytoskeleton modulating the long-range mobility of this protein in the human cell preparation and providing these cells with the ability to recognize microscale separation of the two signaling systems.

The ability of mouse cells to respond to separated CD3-CD28 signaling is associated with higher mobility of Lck. We previously showed that naive mouse lymph node T cells are not sensitive to separation of anti-CD3 and anti-CD28 (13), mounting significant IL-2 secretion on segregated patterns. We attempted to reconcile the sharp contrast in response between these cells and that of resting human cells from peripheral blood. Since the sensitivity of human T cells to micropatterned costimulation was associated with low mobility of Lck relative to deactivation, a reversed balance of these processes might explain the ability of mouse cells to respond to the segregated patterns. In support of this mechanism, Lck-YFP in primary mouse cells on surfaces coated with anti-CD3, anti-CD28, and ICAM/Fc exhibits a long-range diffusion coefficient of 0.37 ± 0.17 $\mu m^2/s$ (mean ± the SD), 8-fold higher than that observed in the human system ($P < 0.001$ compared to human cells, *t* test, 7 to 15 cells per surface). Moreover, pSFK staining for mouse cells on patterned surfaces was distributed across the cell-substrate interface rather than localized to regions of anti-CD3 (Fig. 4A). To further test this model, part of the ICAM/Fc used to coat surfaces was replaced with cholera toxin subunit B (CTX), with the intent of immobilizing GM1 and other membrane components. This approach reduced the diffusion coefficient of Lck-YFP 4-fold to 0.08 ± 0.04 $\mu m^2/s$ (mean ± the SD from 12 cells, $P < 0.001$ compared to non-CTX surface). Inclusion of CTX on these surfaces also increased the correlation of pSFK with regions of anti-CD3 (Fig. 4B and C). Correlation of pSFK with regions of anti-CD28 remained unchanged and largely uncorrelated, a result similar to that discussed for human cells upon treatment with LatB. Finally, inclusion of CTX curtailed IL-2 secretion by cells on the SEG surfaces, mimicking the sensitivity to CD3-CD28 separation observed in human cells (Fig. 4D). IL-2 secretion on CCO surfaces increased on inclusion of CTX on the surface, potentially indicating localized retention of active Lck by the lower mobility (Fig. 4D).

Toward a mechanism for this effect, inclusion of CTX on the surface increased cytoskeletal structure in primary mouse cells

(Fig. 4E), along with cell-substrate contact area (Fig. 4E). However, the per-area intensity of F-actin remained unchanged by this manipulation (Fig. 4E). Wash-in of LatB to cells on CTX-containing surfaces reduced the intensity of phalloidin staining but did not restore Lck mobility (Fig. 4F), suggesting that unlike the human cell system, reduction of Lck mobility by CTX does not involve the cell cytoskeleton. An alternative explanation is that surface-immobilized CTX recruits Lck, via lipid raft domains involving GM1, to the cell-substrate interface. However, CTX slightly decreased the intensity of total Lck staining on both CCO and SEG surfaces (Fig. 4G). This lack of Lck recruitment may be a result of the low density of CTX on the surface; rather than coating the substrate with CTX alone, it was mixed 1:5 with ICAM/Fc. Attachment of CTX to a substrate also restricts the clustering and cross-linking of membrane components that would be observed for such proteins applied in solution. Finally, we note that the CCO surfaces with CTX (Fig. 4D) showed strong IL-2 secretion but the lowest levels of total Lck staining intensity (Fig. 4G); the effect of CTX on cell activation on the SEG surfaces is not simply a result of Lck recruitment.

DISCUSSION

The importance of spatial organization in signaling is suggested by the rich array of cellular structures observed in living tissues. A mechanism for such organization at the multicellular level during morphogenesis was codified by Turing (42), applying the concept of reaction-diffusion systems to the life sciences. In such systems, the concentration of a reactant molecule is expressed not by a single, uniform concentration but is instead locally defined and determined by a variety of factors. These include the presence of sinks and sources, additional reactions that consume or produce this species, and transport throughout the reaction volume which, given the small dimensions of these systems and absent any forced flow, is considered to be diffusion. The practicality of reaction-diffusion mechanisms at subcellular scales was considered in a report by Brown and Kholodenko (14), which included analysis of the phosphorylation state of a freely diffusing signaling molecule that was controlled by a kinase at the surface of a spherical cell and a phosphatase uniformly distributed throughout the cell volume. Based on values of diffusion coefficient, protein activities, and protein concentrations collected from literature, they demonstrated that gradients of phosphorylation can be obtained across practical cell distances of several micrometers. Notably, these models considered cytosolic proteins with diffusion coefficients on the order of 1 to 10 $\mu m^2/s$, higher than those observed for membrane-associated biomolecules, including that of Lck reported here.

We propose that the reaction-diffusion framework provides a plausible model for reconciling the different sensitivities we observed between human T cells from peripheral blood and mouse cells from lymph nodes, based on the mobility of intermediate signaling molecules. Specifically, our data suggest that active Lck is generated at sites of TCR/CD3 engagement and is then transported throughout the cell interface, including areas of CD28 engagement. Whether Lck is still active when it interacts with CD28 is determined by a balance between transport and deactivation; in a system with slow transport (i.e., the human cell system), active Lck is not found far from the areas of CD3 engagement, and CD28 must be within this short range for convergence of these signals. Conversely, a system with fast transport (mouse cells or human cells with destabilized actin networks) will be less sensitive to separation of these two signals. As a feasibility check of our results, we adapted the model of Brown and Kholodenko to a polar geometry, which is more appropriate for events along a cell-substrate interface. Since the lifetime of Y394-phosphorylation for Lck in either system is not known, we adopted a value of 0.1 s^{-1} for the phosphatase activity, within the range identified by Brown and Kholodenko. For a diffusion coefficient of 0.04 $\mu m^2/s$ (corresponding to that for Lck-YFP in the human cell preparation), we predict a 90% decrease in phospho-Lck concentration from a site of phosphorylation to a location 2.5 μm away, the distance between anti-CD3 and anti-CD28 features in the SEG pattern. Conversely, the same model with a diffusion coefficient of 0.3 $\mu m^2/s$ (observed for mouse lymph node cells) predicts a 50% decrease in phospho-Lck concentration over 2 μm, the distance between features in that species-appropriate SEG pattern; the limited extent of the cell-substrate interface would also confine the larger amount of active Lck that diffuses beyond this distance, further concentrating this kinase. These predictions are in keeping with our observations of pSFK staining and the functional output of IL-2 secretion, supporting the proposed reaction-diffusion model.

The question of why Lck exhibits different mobilities in these systems is intriguing. We first considered CD4, a coreceptor found on a range of immune cells and a major binding partner of Lck. However, the diffusion coefficient of CD4, estimated by FRAP using fluorescently labeled Fab fragments, is similar to Lck in each system; mobile CD4 exhibited a diffusion coefficient of 0.26 ± 0.11 $\mu m^2/s$ (mean $\pm$ the SD, $n = 13$ cells) in the mouse system and 0.05 ± 0.03 $\mu m^2/s$ ($n = 21$) for human cells, neither of which were statistically different from Lck ($P < 0.07$ and $P < 0.30$, respectively). Differences in association between Lck and CD4 in the two cell systems would thus not explain the lower mobility observed in the human T cell. Similarly, differential association of Lck with membrane microdomains (30, 43–45) would not explain the differences in mobility, since trapping of GM1 with CTX was required to bring the diffusion coefficient of Lck in mouse cells closer to that of in the human system. We subsequently focused on the cytoskeleton underlying the IS to explain the differences between the mouse and human T-cell systems. Compared to the dense cytoskeletal network observed in the primary human cells (Fig. 3A), artificial synapses formed by mouse cells are much less developed (Fig. 4E and F), potentially posing fewer barriers and less hindrance to Lck mobility. Intriguingly, we note that the concentration of F-actin structures in the IS is typically higher in the outer edge of the cell-substrate interface compared to the center of this structure (2, 46). It is thus possible that cells are more sensitive to spatial separation of TCR/CD3 and CD28 signaling in these denser areas than in the cell center. It is possible that cells are less sensitive to separation of features within the confines of smaller structures such as the cSMAC.

It should be noted that the precise mechanism for CTX action remains unclear. The results presented in Fig. 4F suggest that reduction of Lck mobility by CTX in the mouse system is not related to the cell cytoskeleton. It is attractive to consider immobilization of lipid raft structures as the mechanism for lower protein mobility, but this specific interaction is not strictly required; reorganization of membrane structure by CTX binding (47) or simply immobilization of membrane molecules are also potential mechanisms for these changes.

Differences in cytoskeleton structure may also reconcile the

behavior of primary mouse and human cells observed in a separate context. We recently demonstrated that both types of cells can sense the stiffness of a substrate presenting anti-CD3 and anti-CD28 antibodies (32, 48). However, the range of mechanical stiffness over which modulation of T-cell function was observed was higher in human than mouse cells. Since the cytoskeleton is a central structure in cell mechanobiology, the ability to sense stiffer surfaces by human cells may reflect the more extensive cytoskeleton in that system. It is also recognized that a simple explanation is that species-appropriate anti-CD3 and anti-CD28 (as well as ICAM-1/Fc) are used in each system. However, OKT3 exhibits 4-fold-higher affinity than 145-2C11 (the mouse-reactive counterpart) to CD3 (36, 49); if stronger TCR triggering through higher affinity could overcome the effect of spatial separation, the sensitivity to pattern geometry would have been reversed.

Importantly, it is noted that whereas Lck is the focus of the model developed here, given its central role in T-cell activation, other molecules contribute to CD3-CD28 cross talk. The differences in pSFK distribution between the mouse and human systems and across the various manipulations inspired the reaction-diffusion model and the plausibility of Lck as an important intermediary signaling protein. Such differences were not observed for all signaling molecules. In particular, protein kinase C-θ showed little correlation with areas of CD3 or CD28 engagement in either system (data not shown). It is still possible that Fyn, which would also be detected in our staining for pSFK but is less understood in the context of T-cell activation, provides a complementary function. It is also possible that some other signaling intermediate that is also affected by the mechanisms identified here to modulate Lck diffusion is the true mediator of micropatterned costimulation. A complete methodology for testing the role of a signaling intermediate in a reaction-diffusion system remains to be developed but will be useful in fully resolving our observations and applying this framework to other systems.

The differences in sensitivity to CD28 costimulation geometry and cytoskeletal development contribute to the growing list of recognized differences between mouse and human T-cell physiology (50) but may also explain some of these observations. For example, mouse and human T cells show different patterns of differentiation after activation, such as selection between Th1 versus Th2 lineages, a process governed in part by the balance between different arms of the T-cell activation signaling network. The observation that these two cell types form morphologically different synapses (7) could suggest a role in IS microgeometry in lineage decisions. Finally, the differences in sensitivity to micropatterned costimulation reported here could explain that while the *trans* costimulation is effective in promoting activation of mouse T cells, reports with human cells are more mixed regarding the effectiveness of this configuration (22, 51–53).

Finally, the approach of patterning a cell culture surface with biomolecules (31, 54–58) provides an important counterpart to emerging microscopy techniques that provide unprecedented resolution of biological processes in living cells. Specifically, such patterning allows spatial manipulation of signaling networks with a level of sophistication that is difficult to achieve in other experimental systems. We demonstrate here the use of multicomponent surfaces to provide new insight into a long-standing question in IS function, namely, whether and how the microscale patterns observed in this interface can influence intracellular signaling. Notably, microscale patterning provided near-arbitrary control over synapse layout without modification of the signaling proteins themselves, avoiding secondary effects that are difficult to isolate (25). Micropatterning also provides a level of colocalization or separation between signaling complexes that is difficult to reproduce in cell-cell interfaces; while in this sense nonphysiological, such surfaces provide an important capability for reductionist studies in this new area of signaling research. We anticipate that these experimental and theoretical approaches will provide advanced insight into spatially resolved signaling in a wide range of cellular systems.

ACKNOWLEDGMENTS

We thank R. Sekaly (VGTI Florida) for generously providing the Lck-YFP vector. We also thank Anastasia Liapis of the Dustin lab for her expertise in transfection.

This study was funded by the National Institutes of Health (R01AI088377 and Common Fund Nanomedicine program PN2EY016586) and the National Science Foundation (IGERT 0801530).

The content of this study is solely the responsibility of the authors and does not necessarily represent the official views of the funding institutions.

REFERENCES

1. **Dustin ML, Olszowy MW, Holdorf AD, Li J, Bromley S, Desai N, Widder P, Rosenberger F, van der Merwe PA, Allen PM, Shaw AS.** 1998. A novel adaptor protein orchestrates receptor patterning and cytoskeletal polarity in T-cell contacts. Cell **94:**667–677. http://dx.doi.org/10.1016/S0092-8674(00)81608-6.
2. **Grakoui A, Bromley SK, Sumen C, Davis MM, Shaw AS, Allen PM, Dustin ML.** 1999. The immunological synapse: a molecular machine controlling T cell activation. Science **285:**221–227. http://dx.doi.org/10.1126/science.285.5425.221.
3. **Monks CR, Freiberg BA, Kupfer H, Sciaky N, Kupfer A.** 1998. Three-dimensional segregation of supramolecular activation clusters in T cells. Nature **395:**82–86. http://dx.doi.org/10.1038/25764.
4. **Brossard C, Feuillet V, Schmitt A, Randriamampita C, Romao M, Raposo G, Trautmann A.** 2005. Multifocal structure of the T cell-dendritic cell synapse. Eur. J. Immunol. **35:**1741–1753. http://dx.doi.org/10.1002/eji.200425857.
5. **Purtic B, Pitcher LA, van Oers NSC, Wulfing C.** 2005. T cell receptor (TCR) clustering in the immunological synapse integrates TCR and costimulatory signaling in selected T cells. Proc. Natl. Acad. Sci. U. S. A. **102:**2904–2909. http://dx.doi.org/10.1073/pnas.0406867102.
6. **Singleton KL, Roybal KT, Sun Y, Fu G, Gascoigne NRJ, van Oers NSC, Wulfing C.** 2009. Spatiotemporal patterning during T cell activation is highly diverse. Sci. Signal. **2:**ra15. http://dx.doi.org/10.1126/scisignal.2000199.
7. **Thauland TJ, Koguchi Y, Wetzel SA, Dustin ML, Parker DC.** 2008. Th1 and Th2 cells form morphologically distinct immunological synapses. J. Immunol. **181:**393–399.
8. **Tseng SY, Waite JC, Liu M, Vardhana S, Dustin ML.** 2008. T cell-dendritic cell immunological synapses contain TCR-dependent CD28-CD80 clusters that recruit protein kinase Cθ. J. Immunol. **181:**4852–4863.
9. **Vyas YM, Maniar H, Dupont B.** 2002. Visualization of signaling pathways and cortical cytoskeleton in cytolytic and noncytolytic natural killer cell immune synapses. Immunol. Rev. **189:**161–178. http://dx.doi.org/10.1034/j.1600-065X.2002.18914.x.
10. **Zanin-Zhorov A, Ding Y, Kumari S, Attur M, Hippen KL, Brown M, Blazar BR, Abramson SB, Lafaille JJ, Dustin ML.** 2010. Protein kinase C-theta mediates negative feedback on regulatory T cell function. Science **328:**372–376. http://dx.doi.org/10.1126/science.1186068.
11. **Doh J, Irvine DJ.** 2006. Immunological synapse arrays: patterned protein surfaces that modulate immunological synapse structure formation in T cells. Proc. Natl. Acad. Sci. U. S. A. **103:**5700–5705. http://dx.doi.org/10.1073/pnas.0509404103.
12. **Mossman KD, Campi G, Groves JT, Dustin ML.** 2005. Altered TCR

signaling from geometrically repatterned immunological synapses. Science **310:**1191–1193. http://dx.doi.org/10.1126/science.1119238.
13. **Shen K, Thomas VK, Dustin ML, Kam LC.** 2008. Micropatterning of costimulatory ligands enhances $CD4^+$ T cell function. Proc. Natl. Acad. Sci. U. S. A. **105:**7791–7796. http://dx.doi.org/10.1073/pnas.0710295105.
14. **Brown GC, Kholodenko BN.** 1999. Spatial gradients of cellular phospho-proteins. FEBS Lett. **457:**452–454. http://dx.doi.org/10.1016/S0014-5793(99)01058-3.
15. **Munoz-Garcia J, Kholodenko BN.** 2010. Signaling over a distance: gradient patterns and phosphorylation waves within single cells. Biochem. Soc. Trans. **38:**1235–1241. http://dx.doi.org/10.1042/BST0381235.
16. **Neves SR, Iyengar R.** 2009. Models of spatially restricted biochemical reaction systems. J. Biol. Chem. **284:**5445–5449.
17. **Neves SR, Tsokas P, Sarkar A, Grace EA, Rangamani P, Taubenfeld SM, Alberini CM, Schaff JC, Blitzer RD, Moraru II, Iyengar R.** 2008. Cell shape and negative links in regulatory motifs together control spatial information flow in signaling networks. Cell **133:**666–680. http://dx.doi.org/10.1016/j.cell.2008.04.025.
18. **Ding L, Shevach EM.** 1994. Activation of CD4+ T cells by delivery of the B7 costimulatory signal on bystander antigen-presenting cells (transcostimulation). Eur. J. Immunol. **24:**859–866. http://dx.doi.org/10.1002/eji.1830240413.
19. **Jenkins MK, Ashwell JD, Schwartz RH.** 1988. Allogeneic non-T spleen cells restore the responsiveness of normal T cell clones stimulated with antigen and chemically modified antigen-presenting cells. J. Immunol. **140:**3324–3330.
20. **Mandelbrot DA, Kishimoto K, Auchincloss H, Jr, Sharpe AH, Sayegh MH.** 2001. Rejection of mouse cardiac allografts by costimulation in trans. J. Immunol. **167:**1174–1178.
21. **Sanchez-Lockhart M, Miller J.** 2006. Engagement of CD28 outside of the immunological synapse results in upregulation of IL-2 mRNA stability but not IL-2 transcription. J. Immunol. **176:**4778–4784.
22. **Smythe JA, Fink PD, Logan GJ, Lees J, Rowe PB, Alexander IE.** 1999. Human fibroblasts transduced with CD80 or CD86 efficiently *trans*-costimulate $CD4^+$ and $CD8^+$ T lymphocytes in HLA-restricted reactions: implications for immune augmentation cancer therapy and autoimmunity. J. Immunol. **163:**3239–3249.
23. **Andres PG, Howland KC, Dresnek D, Edmondson S, Abbas AK, Krummel MF.** 2004. CD28 signals in the immature immunological synapse. J. Immunol. **172:**5880–5886.
24. **Yokosuka T, Kobayashi W, Sakata-Sogawa K, Takamatsu M, Hashimoto-Tane A, Dustin ML, Tokunaga M, Saito T.** 2008. Spatiotemporal regulation of T cell costimulation by TCR-CD28 microclusters and protein kinase C θ translocation. Immunity **29:**589–601. http://dx.doi.org/10.1016/j.immuni.2008.08.011.
25. **Tseng S-Y, Liu M, Dustin ML.** 2005. CD80 cytoplasmic domain controls localization of CD28, CTLA-4, and protein kinase C-θ in the immunological synapse. J. Immunol. **175:**7829–7836.
26. **Raab M, Cai YC, Bunnell SC, Heyeck SD, Berg LJ, Rudd CE.** 1995. p56Lck and p59Fyn regulate CD28 binding to phosphatidylinositol 3-kinase, growth factor receptor-bound protein GRB-2, and T cell-specific protein-tyrosine kinase ITK: implications for T-cell costimulation. Proc. Natl. Acad. Sci. U. S. A. **92:**8891–8895. http://dx.doi.org/10.1073/pnas.92.19.8891.
27. **van Oers NS.** 1999. T cell receptor-mediated signs and signals governing T cell development. Semin. Immunol. **11:**227–237. http://dx.doi.org/10.1006/smim.1999.0179.
28. **Ehrlich LI, Ebert PJ, Krummel MF, Weiss A, Davis MM.** 2002. Dynamics of p56lck translocation to the T cell immunological synapse following agonist and antagonist stimulation. Immunity **17:**809–822. http://dx.doi.org/10.1016/S1074-7613(02)00481-8.
29. **Holdorf AD, Lee KH, Burack WR, Allen PM, Shaw AS.** 2002. Regulation of Lck activity by CD4 and CD28 in the immunological synapse. Nat. Immunol. **3:**259–264. http://dx.doi.org/10.1038/ni761.
30. **Tavano R, Gri G, Molon B, Marinari B, Rudd CE, Tuosto L, Viola A.** 2004. CD28 and lipid rafts coordinate recruitment of Lck to the immunological synapse of human T lymphocytes. J. Immunol. **173:**5392–5397.
31. **Shi P, Shen K, Kam L.** 2007. Local presentation of L1 and N-cadherin in multicomponent, microscale patterns differentially direct neuron function in vitro. Dev. Neurobiol. **67:**1765–1776. http://dx.doi.org/10.1002/dneu.20553.
32. **Judokusumo E, Tabdanov E, Kumari S, Dustin ML, Lance Kam C.** 2012. Mechanosensing in T lymphocyte activation. Biophys. J. **102:**L5–L7. http://dx.doi.org/10.1016/j.bpj.2011.12.011.
33. **Sharif-Askari E, Gaucher D, Halwani R, Ma J, Jao K, Abdallah A, Haddad EK, Sekaly RP.** 2007. p56Lck tyrosine kinase enhances the assembly of death-inducing signaling complex during Fas-mediated apoptosis. J. Biol. Chem. **282:**36048–36056. http://dx.doi.org/10.1074/jbc.M706007200.
34. **Jonsson P, Jonsson MP, Tegenfeldt JO, Hook F.** 2008. A method improving the accuracy of fluorescence recovery after photobleaching analysis. Biophys. J. **95:**5334–5348. http://dx.doi.org/10.1529/biophysj.108.134874.
35. **Baroja ML, Lorre K, Van Vaeck F, Ceuppens JL.** 1989. The anti-T cell monoclonal antibody 9.3 (anti-CD28) provides a helper signal and bypasses the need for accessory cells in T cell activation with immobilized anti-CD3 and mitogens. Cell. Immunol. **120:**205–217. http://dx.doi.org/10.1016/0008-8749(89)90188-3.
36. **Burns GF, Boyd AW, Beverley PC.** 1982. Two monoclonal anti-human T lymphocyte antibodies have similar biologic effects and recognize the same cell surface antigen. J. Immunol. **129:**1451–1457.
37. **James JR, Vale RD.** 2012. Biophysical mechanism of T-cell receptor triggering in a reconstituted system. Nature **487:**64–69. http://dx.doi.org/10.1038/nature11220.
38. **Varma R, Campi G, Yokosuka T, Saito T, Dustin ML.** 2006. T cell receptor-proximal signals are sustained in peripheral microclusters and terminated in the central supramolecular activation cluster. Immunity **25:**117–127. http://dx.doi.org/10.1016/j.immuni.2006.04.010.
39. **Douglass AD, Vale RD.** 2005. Single-molecule microscopy reveals plasma membrane microdomains created by protein-protein networks that exclude or trap signaling molecules in T cells. Cell **121:**937. http://dx.doi.org/10.1016/j.cell.2005.04.009.
40. **Zimmermann L, Paster W, Weghuber J, Eckerstorfer P, Stockinger H, Schutz GJ.** 2010. Direct observation and quantitative analysis of Lck exchange between plasma membrane and cytosol in living T cells. J. Biol. Chem. **285:**6063–6070. http://dx.doi.org/10.1074/jbc.M109.025981.
41. **Ike H, Kosugi A, Kato A, Iino R, Hirano H, Fujiwara T, Ritchie K, Kusumi A.** 2003. Mechanism of Lck recruitment to the T-cell receptor cluster as studied by single-molecule-fluorescence video imaging. ChemPhysChem **4:**620–626. http://dx.doi.org/10.1002/cphc.200300670.
42. **Turing AM.** 1952. The chemical basis of morphogenesis. Philos. Trans. R. Soc. London. Ser. B Biol. Sci. **237:**37–72. http://dx.doi.org/10.1098/rstb.1952.0012.
43. **Filipp D, Zhang J, Leung BL, Shaw A, Levin SD, Veillette A, Julius M.** 2003. Regulation of Fyn through translocation of activated Lck into lipid rafts. J. Exp. Med. **197:**1221–1227. http://dx.doi.org/10.1084/jem.20022112.
44. **Irles C, Arias-Martinez J, Guzman-Barcenas J, Ortega A.** 2010. Plasma membrane subdomain partitioning of Lck in primary human T lymphocytes. Can. J. Physiol. Pharmacol. **88:**487–496. http://dx.doi.org/10.1139/Y09-125.
45. **Stefanova I, Horejsi V, Ansotegui IJ, Knapp W, Stockinger H.** 1991. GPI-anchored cell-surface molecules complexed to protein tyrosine kinases. Science **254:**1016–1019. http://dx.doi.org/10.1126/science.1719635.
46. **Babich A, Li S, O'Connor RS, Milone MC, Freedman BD, Burkhardt JK.** 2012. F-actin polymerization and retrograde flow drive sustained PLCγ1 signaling during T cell activation. J. Cell Biol. **197:**775–787. http://dx.doi.org/10.1083/jcb.201201018.
47. **Hammond AT, Heberle FA, Baumgart T, Holowka D, Baird B, Feigenson GW.** 2005. Cross-linking a lipid raft component triggers liquid ordered-liquid disordered phase separation in model plasma membranes. Proc. Natl. Acad. Sci. U. S. A. **102:**6320–6325. http://dx.doi.org/10.1073/pnas.0405654102.
48. **O'Connor RS, Hao X, Shen K, Bashour K, Akimova T, Hancock WW, Kam LC, Milone MC.** 2012. Substrate rigidity regulates human T cell activation and proliferation. J. Immunol. **189:**1330–1339. http://dx.doi.org/10.4049/jimmunol.1102757.
49. **Portoles P, Rojo J, Golby A, Bonneville M, Gromkowski S, Greenbaum L, Janeway CA, Jr, Murphy DB, Bottomly K.** 1989. Monoclonal antibodies to murine CD3 epsilon define distinct epitopes, one of which may interact with CD4 during T cell activation. J. Immunol. **142:**4169–4175.
50. **Mestas J, Hughes CCW.** 2004. Of mice and not men: differences between mouse and human immunology. J. Immunol. **172:**2731–2738.
51. **Cardoso AA, Seamon MJ, Afonso HM, Ghia P, Boussiotis VA, Freeman GJ, Gribben JG, Sallan SE, Nadler LM.** 1997. Ex vivo generation of human anti-pre-B leukemia-specific autologous cytolytic T cells. Blood **90:**549–561.

52. **Liu Y, Janeway CA.** 1992. Cells that present both specific ligand and costimulatory activity are the most efficient inducers of clonal expansion of normal CD4 T cells. Proc. Natl. Acad. Sci. U. S. A. **89:**3845–3849. http://dx.doi.org/10.1073/pnas.89.9.3845.
53. **Van de Veide H, Lorré K, Bakkus M, Thielemans K, Ceuppens JL, de Boer M.** 1993. CD45RO$^+$ memory T cells but not CD45RA$^+$ naive T cells can be efficiently activated by remote costimulation with B7. Intern. Immunol. **5:**1483–1487. http://dx.doi.org/10.1093/intimm/5.11.1483.
54. **Borghi N, Lowndes M, Maruthamuthu V, Gardel ML, Nelson WJ.** 2010. Regulation of cell motile behavior by crosstalk between cadherin- and integrin-mediated adhesions. Proc. Natl. Acad. Sci. U. S. A. **107:**13324–13329. http://dx.doi.org/10.1073/pnas.1002662107.
55. **Chen CS, Mrksich M, Huang S, Whitesides GM, Ingber DE.** 1997. Geometric control of cell life and death. Science **276:**1425–1428. http://dx.doi.org/10.1126/science.276.5317.1425.
56. **Desai RA, Khan MK, Gopal SB, Chen CS.** 2011. Subcellular spatial segregation of integrin subtypes by patterned multicomponent surfaces. Integr. Biol. **3:**560–567. http://dx.doi.org/10.1039/c0ib00129e.
57. **Orth RN, Wu M, Holowka DA, Craighead HG, Baird BA.** 2003. Mast cell activation on patterned lipid bilayers of subcellular dimensions. Langmuir **19:**1599–1605. http://dx.doi.org/10.1021/la026314c.
58. **Tsai J, Kam L.** 2009. Rigidity-dependent cross talk between integrin and cadherin signaling. Biophys. J. **96:**L39–L41. http://dx.doi.org/10.1016/j.bpj.2009.01.005.